Generation of highly pure pluripotent stem cell-derived myogenic progenitor cells and myotubes

Reem Bou Akar, Chéryane Lama, Déborah Aubin, Julien Maruotti, Brigitte Onteniente, Joana Esteves de Lima, Frédéric Relaix

Stem Cell Reports
Article

ISSCR

OPEN ACCESS

Generation of highly pure pluripotent stem cell-derived myogenic progenitor cells and myotubes

Reem Bou Akar,[1] Chéryane Lama,[1] Déborah Aubin,[2] Julien Maruotti,[2] Brigitte Onteniente,[2] Joana Esteves de Lima,[1,3] and Frédéric Relaix[1,3,*]

[1]University Paris Est Creteil, INSERM, EnvA, EFS, AP-HP, IMRB, 94010 Creteil, France
[2]PHENOCELL SAS, 06130 Grasse, France
[3]Co-senior author
*Correspondence: frederic.relaix@inserm.fr
https://doi.org/10.1016/j.stemcr.2023.11.002

SUMMARY

Driving efficient and pure skeletal muscle cell differentiation from pluripotent stem cells (PSCs) has been challenging. Here, we report an optimized protocol that generates skeletal muscle progenitor cells with high efficiency and purity in a short period of time. Human induced PSCs (hiPSCs) and murine embryonic stem cells (mESCs) were specified into the mesodermal myogenic fate using distinct and species-specific protocols. We used a specific maturation medium to promote the terminal differentiation of both human and mouse myoblast populations, and generated myotubes associated with a large pool of cell-cycle arrested PAX7$^+$ cells. We also show that myotube maturation is modulated by dish-coating properties, cell density, and percentage of myogenic progenitor cells. Given the high efficiency in the generation of myogenic progenitors and differentiated myofibers, this protocol provides an attractive strategy for tissue engineering, modeling of muscle dystrophies, and evaluation of new therapeutic approaches *in vitro*.

INTRODUCTION

Skeletal muscle plays a fundamental role in locomotion, generation of body heat, oxygen consumption, and metabolism. Skeletal muscle derives from transient epithelial structures, the somites, which are formed through repetitive segmentation of the paraxial mesoderm during development (Buckingham and Rigby, 2014). The somites give rise to the sclerotome, the syndetome, and the dermomyotome. The dermomyotome forms the skeletal muscles of the trunk and limbs and expresses the paired-box transcription factor PAX3, a key upstream regulator of myogenesis, and the center of the dermomyotome coexpresses PAX7. In the mouse, myogenesis is initiated at embryonic day 9.5 (E9.5) in the dermomyotome cells that upregulate the expression of the myogenic regulatory factor (MRF) MYF5 and migrate ventrally to form the myotome (Buckingham and Rigby, 2014; Esteves de Lima and Relaix, 2021). The PAX3$^+$ cells commit to the myogenic lineage by activating the expression of the basic helix-loop-helix MRFs MYF5, MYOD, and MRF4 and undergo terminal differentiation with the expression of the differentiation marker myogenin (MYOG). Murine myogenesis occurs in 2 successive and overlapping phases: the embryonic, in which PAX3$^+$ muscle progenitors differentiate and fuse, giving rise to the first fibers, and the fetal, which relies on PAX7$^+$ progenitor cells (Messina and Cossu, 2009). During fetal myogenesis, muscle growth is accomplished by the fusion of PAX7$^+$ progenitor-derived myoblasts, which are characterized by the expression of NFIX, resulting in myofibers that express MYH3 and MYH8 (Messina et al., 2010; Schiaffino et al., 2015). By the end of fetal myogenesis, PAX7$^+$ cells adopt a satellite cell position under the basal lamina of the fiber and progressively exit cell cycle and become quiescent (Buckingham and Rigby, 2014; Esteves de Lima et al., 2014; Picard and Marcelle, 2013). These cells mediate postnatal growth and muscle repair. Human myogenesis occurs in 3 successive and overlapping waves. Primary myogenesis is initiated at week 8 of gestation, establishing the muscle pattern and primary myofibers expressing the embryonic myosin heavy chain (MHC) (MYH3), followed by the slow (MYH7) and the neonatal (MYH8) MHC (Barbet et al., 1991; Draeger et al., 1987). Secondary myogenesis starts at week 10 and is critical for the growth and maturation of skeletal muscle. At this phase, myofibers express MYH3 at week 12 and at later stages, MYH8 (Cho et al., 1993). After week 27, secondary fibers expresses MYH7, and by week 30, ~50% of all muscle fibers are MYH7$^+$. A tertiary fiber population at weeks 16–17 contributes to postnatal growth and repair of damaged muscle. Initially, tertiary myogenesis is composed of very small myofibers expressing adult fast but not neonatal MHC (Draeger et al., 1987; Ecob-Prince et al., 1989). *MYH2* transcripts are weakly expressed at week 19 and strongly expressed at birth, whereas *MYH1* transcripts become strongly expressed 30 days after birth.

Recapitulation of myogenesis *in vitro* has been widely studied; however, it remains a challenge to obtain a pure and mature myogenic population from pluripotent stem cells (PSCs). Several studies described the generation of myogenic cells from murine embryonic stem cells (mESCs) and human induced PSCs (hiPSCs) using transgene and transgene-free methods. The overexpression of master regulators such as

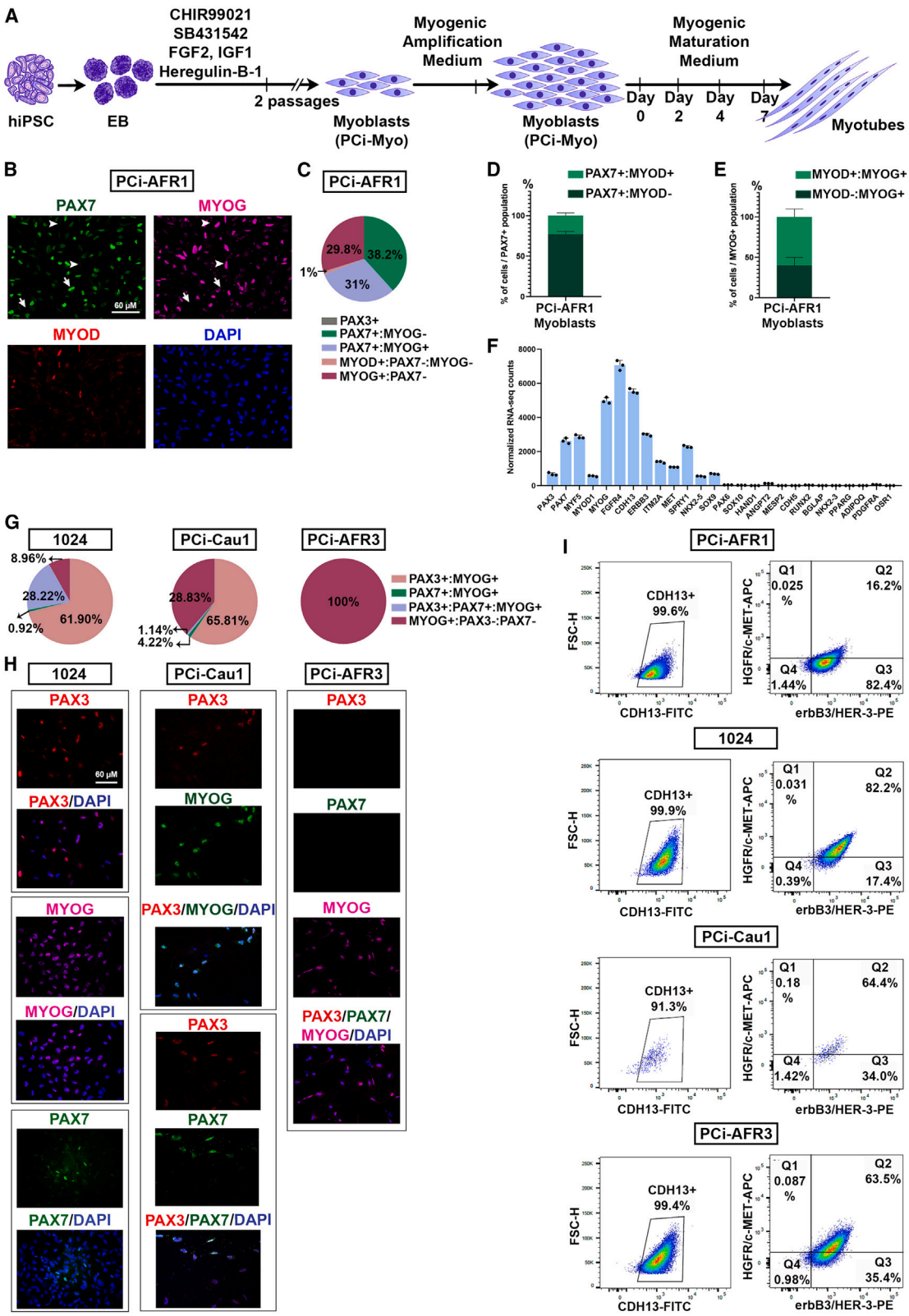

(legend on next page)

PAX3, PAX7, and MYOD efficiently differentiate PSCs into the myogenic lineage (Abujarour et al., 2014; Akiyama et al., 2018; Albini et al., 2013; Darabi et al., 2008, 2011; Dekel et al., 1992; Sato et al., 2019; Tanaka et al., 2013; Tedesco et al., 2012; Warren et al., 2010). Such methods are useful for drug screening, *in vitro* muscle disease modeling, and functional testing. However, the progenitor state is bypassed in the analysis. Alternative transgene-free protocols involve the stepwise addition of molecules and growth factors to the culture medium to favor myogenic differentiation (Caron et al., 2016; Chal et al., 2015; Choi et al., 2016; Hicks et al., 2018; Shelton et al., 2016). These directed differentiation methods provide a more accurate tool to study myogenesis *in vitro*. However, myogenic differentiation based on the modulation of medium composition is challenging due to contamination by other cell types.

In this study, we describe a protocol that specifically produces myogenic progenitors and differentiated myotubes from hiPSCs and mESCs. This protocol is based on a 2-dimensional (2D) culture system, in which the cells are treated with defined components, successfully driving myogenic differentiation, myoblast fusion, and the establishment of a reserve population. Of note, the described myogenic protocol enables the production of highly enriched myogenic cultures quickly and without the need for cell sorting.

RESULTS

Differentiation of hiPSC into myoblasts

To differentiate the hiPSC-AFR1 line into the myogenic lineage, embryoid bodies (EBs) (Shevde and Mael, 2013) were plated on Geltrex-coated dishes, a commercial soluble form of basement membrane, in the complete myogenic medium supplemented with the Wnt activator CHIR99021, the transforming growth factor-β (TGF-β) inhibitor SB431542, fibroblast growth factor-2 (FGF2), insulin growth factor-1 (IGF1), and heregulin-β-1 (Figure 1A). The EB expressed the early mesodermal marker brachyury (T-box transcription factor T) at day 2, followed by the coexpression of PAX3 and PAX7 at days 8 and 12 (Figure S1A). The cells lost PAX3 expression by day 14 and expressed PAX7, which was maintained until day 18 (Figure S1A). These results suggest that the EB-derived cells progressed through presomitic mesoderm and dermomyotomal differentiation. At day 18, we obtained a precursor cell population that was maintained for 2 additional passages in the same medium to enrich for the final PCi-AFR1-derived myoblast population (PCi-Myo). At this stage, the cells can be stored for banking or triggered to differentiate. To amplify the PCi-Myo population, the cells were cultured in a specific amplification medium that contains FGF2, IGF1, heregulin-β-1, and forskolin (Figure 1A).

PCi-Myo derived from hiPSC-AFR1 was seeded at low confluence (25,000 cells/cm^2) in amplification medium (Figure 1A). This myogenic population proliferates at the rate of 1.8 cycles every 24 h and can be expanded up to 5 passages. This population was defined by 38.2% (±11.1) of PAX7$^+$ cells (progenitor cells), 31% (±10.3) PAX7^{Low}:MYOG-double-positive cells, 29.8% (±1.1) PAX7-:MYOG$^+$ cells, and 1% (±0.3) MYOD$^+$ cells (Figures 1B and 1C; Table S1). MYOD was coexpressed in 22.9% of the PAX7$^+$ cells and in 59.9% of the MYOG$^+$ cells (Figures 1D and 1E). qRT-PCR analysis confirmed that PCi-Myo express *PKC*-θ, *MCK*, and *ITGA7* (Figure S1B), genes associated with fetal myoblasts (Biressi et al., 2007a, b). Immunostainings showed that 100% of the PCi-Myo were myogenic (Figures 1C and S2A; Table S1). To further validate the purity of these cells, we performed RNA sequencing (RNA-seq) on PCi-Myo (myoblasts) and confirmed the increased expression of myogenic genes such as *PAX3*, *PAX7*, *FGFR4*, and *CDH13*, whereas markers

Figure 1. Characterization of the human skeletal myoblasts generated from hiPSCs

(A) Schematic representation of the experimental time line.

(B) Immunostaining with PAX7, MYOD, MYOG, and DAPI staining in PCi-AFR1-derived PCi-Myo cells, cultured on Geltrex-coated dishes. Arrows indicate PAX7$^+$:MYOG$^-$ cells and arrowheads indicate PAX7$^-$:MYOG$^+$ cells. Scale bar, 60 μM.

(C) Quantification of the cell populations in the whole culture dish at the amplification stage (PCi-AFR1-derived PCi-Myo) cultured on Geltrex-coated dishes (n = 3, independent experiments).

(D and E) Quantification of the (D) PAX7$^+$:MYOD$^-$ and PAX7$^+$:MYOD$^+$ cells within the PAX7$^+$ cell population and (E) MYOD$^+$:MYOG$^+$ and MYOD$^-$:MYOG$^+$ cells within the MYOG$^+$ cell population, at the amplification stage (PCi-AFR1-derived PCi-Myo) on Geltrex-coated dishes (n = 3, independent experiments). Error bars, mean ± SEM.

(F) Histogram with the normalized reads per gene of PCi-AFR1-derived PCi-Myo RNA-seq data in individual triplicates. Error bars, mean ± SEM.

(G) Quantification of the cell populations in the whole culture dish at the amplification stage (1024/PCi-Cau1/PCi-AFR3-derived myoblasts) cultured on Geltrex-coated dishes (n = 3, independent experiments).

(H) Immunostaining with PAX3, PAX7, MYOG, and DAPI staining in 1024/PCi-Cau1/PCi-AFR3-derived myoblasts, cultured on Geltrex-coated dishes. Scale bar, 60 μM.

(I) Flow cytometry analysis of PCi-AFR1/1024/PCi-Cau1/PCi-AFR3-derived myoblasts, cultured on Geltrex-coated dishes, for CDH13, erbB3/HER, and HGFR/c-met expression.

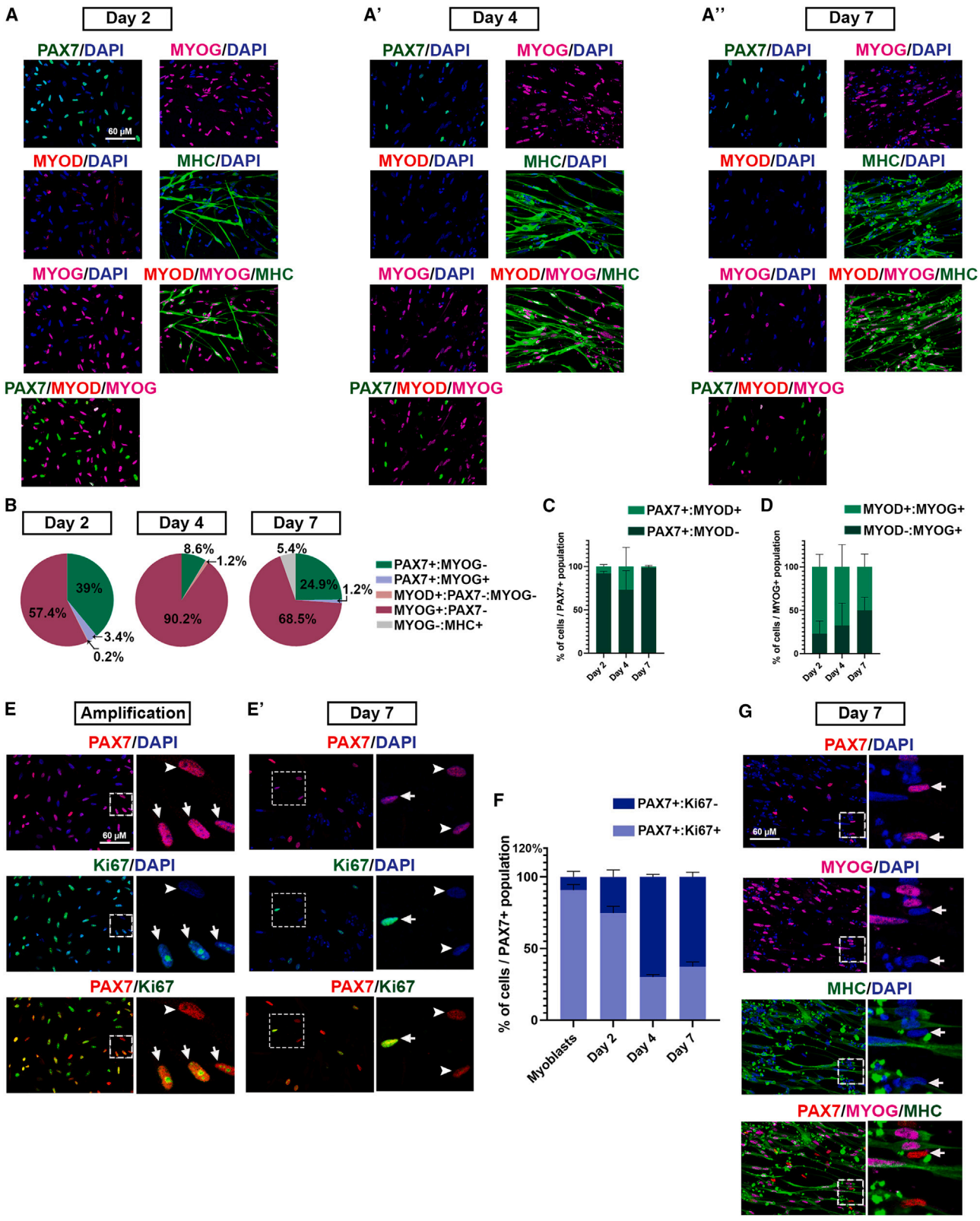

(legend on next page)

from other lineages had low or absent expression (genes such as *PAX6*, *PDGFRA*, *RUNX2*, and *CDH5*) (Figure 1F; Table S1).

To assess the protocol's reproducibility, we performed it on 3 other cell lines. Strikingly, although hiPSC-AFR1 needed to pass through an EB-formation step to achieve myogenic differentiation, the other tested lines, hiPSC-1024, PCi-Cau1, and PCi-AFR3, only required detachment with accutase at 80% confluence and subsequent culture in complete myogenic medium for 18 days to yield PCi-Myo. Immunostainings for PAX3, PAX7, and MYOG showed that the 3 cell lines originated pure myogenic populations but expressed distinct combinations of myogenic factors (Figures 1G, 1H, S2B–S2D; Table S1). We further analyzed by flow cytometry the expression of myogenic surface markers CDH13, ERBB3, and HGFR (Hicks et al., 2018; Nalbandian et al., 2021) in the hiPSC-derived myoblast populations. We found that over 90% of the myoblasts derived from 4 distinct hiPSC lines expressed CDH13 (Figures 1I and S1C). Moreover, more than 80% of the PCi-AFR1-derived CDH13$^+$ cells coexpressed ERBB3, whereas the CDH13$^+$ populations derived from PCI-AFR3, PCi-Cau1, and 1024 were mostly double-positive for ERBB3 and HGFR (Figure 1I). These results confirm that the 4 populations derived from distinct hiPSC lines are enriched in myogenic cells, despite the heterogeneity associated with the myogenic markers that they express.

Differentiation of hiPSC-derived myoblasts into myotubes

To induce terminal myogenic differentiation, we seeded the PCi-MYO on Geltrex- or laminin-coated dishes at a high density (100,000 cells/cm^2). PCi-MYO cells were cultured with maturation medium obtained from (PhenoCULT-MYO, Phenocell) to promote differentiation and fusion of the myoblasts into multinucleated myotubes (Figure 1A). After 2 days of culture in maturation medium (day 2), the percentage of MYOG$^+$ cells increased to 57.4% (±4.3), reaching a maximum at day 4 (90.2% ± 1.3%) (Figures 2A, 2A′, and 2B). By contrast, the percentage of PAX7$^+$ cells decreased between days 2 and 4, from 39% (±2.3) to 8.6% (±2.4) (Figures 2A, 2A′, and 2B). Thereafter, the PAX7$^+$ population increased and constituted 24.9% (±6.8) of the cells at day 7 (Figures 1A″ and 1B).

The myogenic commitment marker MYOD was mostly associated with the terminal differentiation marker MYOG throughout differentiation (Figures 2A, 2A′, 2A″, 2C, and 2D). The PAX7$^+$:MYOD$^+$ subpopulation increased to reach 26.8% of all PAX7$^+$ cells at day 4, but it was no longer observed at day 7 (Figures 2A′, 2A″, and 2C).

To confirm the myogenic purity of the cultures during differentiation, we performed immunostaining for nonmyogenic markers, such as SOX2, CD31, and PDGFRα at day 7 (Figures S3A, S3A′, S3A″, and S3A‴). Consistently, qRT-PCR results revealed that the expression level of nonmuscle genes was lower in hiPSC-derived myotubes than the ones derived from primary cultures (Figures S3B–S3D).

The number of PAX7$^+$ cells increased from days 4 to 7 (Figures 2A′, 2A″, and 2B), demonstrating that these culture conditions stimulate the generation of myogenic progenitor cells. During the amplification phase, 91% of the PAX7$^+$ cells were proliferative, as observed with the cell-cycle marker KI67 (Figures 2E and 2F). By day 2, the proliferating PAX7$^+$ cell number decreased, and at day 7, 62.7% of the PAX7$^+$ cells were in growth arrest (Figures 2E′ and 2F). At late differentiation stages, the nonproliferative PAX7$^+$ cells were found near the myotubes (Figure 2G). These cells constitute a reserve cell population that was not observed when differentiating hiPSC into myogenic cells using commercial mediums (https://www.amsbio.com/skeletal-muscle-differentiation/) associated with the previously published transgene-free protocol (Caron et al., 2016) (Figures S4A and S4A′).

Next, we investigated whether the reserve cells were able to regenerate muscles *in vivo* by grafting 500 × 10^3 cells in $BaCl_2$-injured tibialis anterior (TA) muscles of

Figure 2. Characterization of the human skeletal myotubes and PAX7$^+$ cells, generated from hiPSC PCi-AFR1 at day 7

(A, A′, A″) Left: immunostaining with PAX7, MYOD, MYOG, and DAPI staining in PCi-MYO cells. Right: immunostaining with MYOG and MHC and DAPI staining in PCi-AFR1-derived PCi-MYO cells at day 2 (A), day 4 (A′), and day 7 (A″), cultured on Geltrex-coated dishes. Scale bar, 60 μM.

(B) Quantification of the cell populations in the whole-cell culture dish at the amplification stage (myoblasts) and during differentiation with Phenocell maturation medium (days 2, 4, and 7), cultured on Geltrex-coated dishes (n = 3, independent experiments).

(C and D) Quantification of the (C) PAX7$^+$:MYOD$^-$ and PAX7$^+$:MYOD$^+$ cells within the PAX7$^+$ cell population and (D) MYOD$^+$:MYOG$^+$ and MYOD$^-$:MYOG$^+$ cells within the MYOG$^+$ cell population, during PCi-AFR1-derived myoblasts differentiation with Phenocell maturation medium (days 2, 4, and 7) on Geltrex-coated dishes (n = 3, independent experiments). Error bars, mean ± SEM.

(E and E′) Immunostaining with PAX7, KI67, and DAPI staining in PCi-AFR1 PCi-MYO cells at the amplification stage (myoblasts) (E) and at day 7 (E′) cultured on Geltrex-coated dishes. Arrows indicate PAX7$^+$:KI67$^+$ cells and arrowheads indicate PAX7$^+$:KI67$^-$ cells. Scale bar, 60 μM.

(F) Quantification of the PAX7$^+$:KI67$^+$ and PAX7$^+$:KI67$^-$ cells within the PAX7$^+$ cell population at the amplification stage (myoblasts) and during differentiation with maturation medium (days 2, 4, and 7) (n = 3, independent experiments). Error bars, mean ± SEM.

(G) Immunostaining with PAX7, MYOG, MHC, and DAPI staining in PCi-MYO cells at day 7 cultured on Geltrex-coated dishes. Arrows indicate PAX7$^+$ cells. Scale bar, 60 μM.

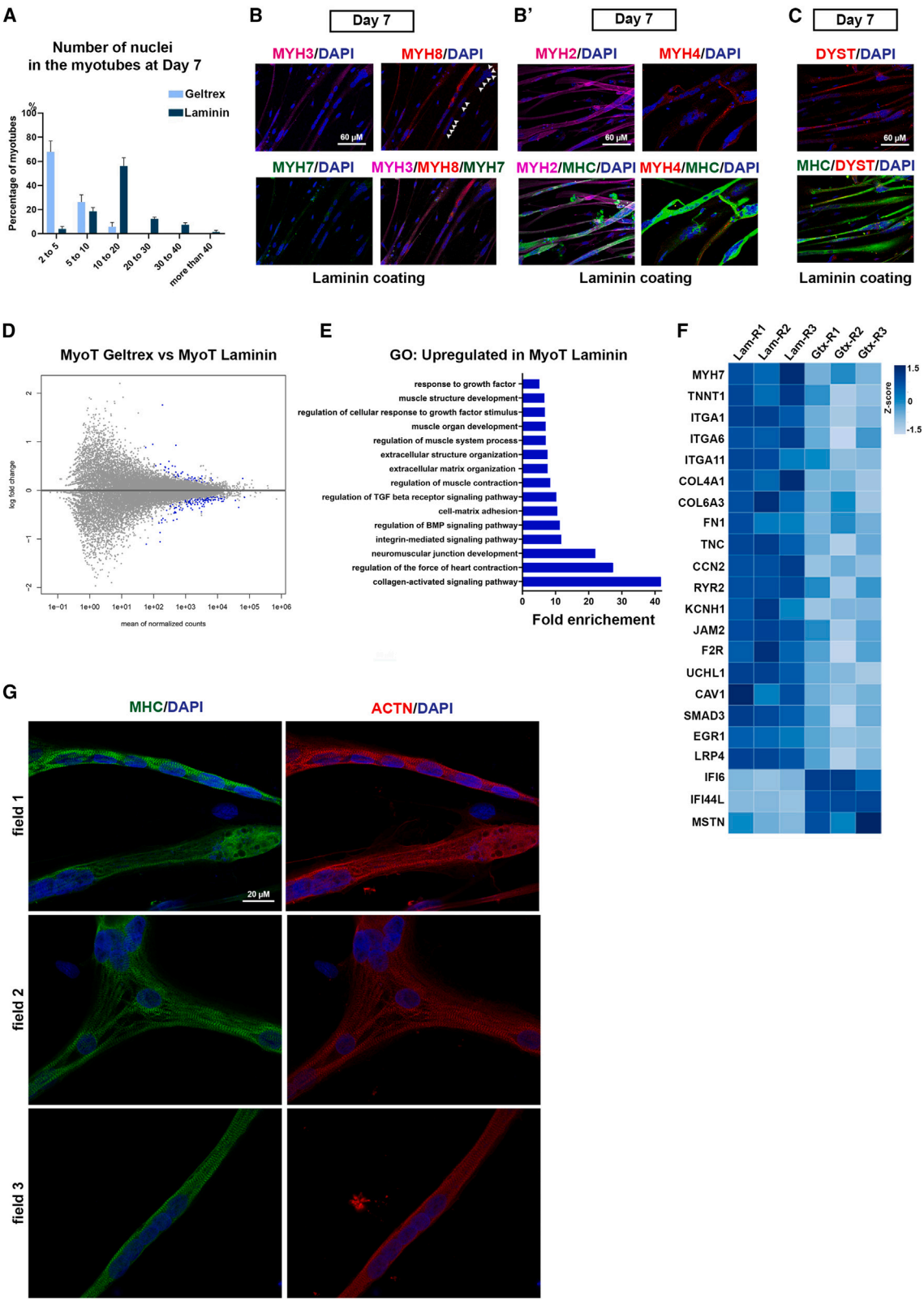

(legend on next page)

immunodeficient Rag2$^{-/-}$:γc$^{-/-}$ mice. The contralateral TA was grafted with 500 × 10^3 CD56$^+$ human myoblasts isolated from human muscle biopsies as control. Although we detected a few human LAMINA/C$^+$ myonuclei in the fibers of the TA grafted with hiPSC-derived PAX7$^+$ reserve cells (Figures S4B, S4E, and S4F), we found more human nuclei in the TA grafted with primary myoblasts (Figures S4C and S4D). Therefore, the hiPSC-derived PAX7$^+$ reserve cells showed a limited regenerative capacity in the murine host.

Characterization of the hiPSC-derived myotubes

The first fusion events occurred between days 2 and 4 of PCi-Myo culture in maturation medium (Figures 2A, 2A′, and S5A). We tested different dish coatings and compared the culture of PCi-Myo on laminin- versus Geltrex-coated dishes. PCi-Myo cultured on laminin underwent differentiation kinetics similar to those cultured on Geltrex, but displayed larger myotubes at day 7 (Figures 3 and S5A′). A total of 60% of the myotubes cultured on laminin contained 10 to 20 nuclei (Figures 3A and 3B) versus 70% of myotubes cultured on Geltrex that displayed 2–5 nuclei (Figures 3A and S5A′). The myotubes obtained on Geltrex coating at days 4 and 7 were characterized mainly by the expression of the embryonic (MYH3) and fetal MHCs (MYH8) (Figures S5A and S5A′). Only a few myotubes expressed the adult slow MHC isoform (MYH7) at day 7 (Figure S5A″). By contrast, the myotubes obtained on laminin coating at day 7 expressed a mix of the fetal (MYH8), adult slow (MYH7), and adult fast type IIa (MYH2) and type IIb (MYH4) MHC isoforms (Figures 3B and 3B′). Dystrophin was detected at day 7 in the myotubes differentiated on Geltrex- and laminin-coated dishes (Figures 3C and S5B). RNA-seq experiments further confirmed these results (Figures 3D and S5C). We observed that the myotubes plated on laminin displayed a more mature phenotype compared to those plated on Geltrex, with higher expression of myotube-maturation genes such as *MYH7*, *TNNT1*, *CAV1*, *KCNH1*, *TNC*, *CTGF*, *ITGA1*, *ITGA6*, and *ITGA11* (Figures 3E and 3F). More important, hiPSC-derived myotubes obtained on laminin coating displayed organized sarcomeres, demonstrated by α-actinin immunostaining (Figure 3G). These results were supported by qRT-PCR, where the expression levels of genes that code for triad subunits such as *DHPRα*, *DHPRβ*, *DHPRγ*, *ATP2A1*, *CASQ1*, *SCN4A*, and *SCN5A* (Figures S5D, S5D′, S5D″, and S5E) were higher in laminin-coated cultures. Taken together, the higher myotube maturity level on laminin-coated dishes highlights the importance of the dish coating in differentiation.

Optimization of the mESC paraxial mesodermal differentiation protocol to obtain myogenic progenitors

In vivo fundamental research is highly linked to the use of mice as a model organism. Consequently, we established a similar protocol to drive mESCs into myogenic differentiation. We differentiated mESCs into paraxial mesoderm by adapting the protocol from Chal et al. (2018) (Figure 4A). At day 4, the mESCs exhibited a posterior presomitic mesodermal fate characterized by the expression of brachyury (T) (Figure 4B), *Msgn1*, and *Tbx6* (Figure 4E). To promote the progression to anterior presomitic mesodermal differentiation, the cells were cultured in a serum-free medium for 2 additional days, containing the same molecules described above (days 4–6) (Figure 4A), leading to the expression of *Pax3*, *Pax7*, and *Pdgfra* (Figure 4E). By day 6, 27.6% of the cells expressed the anterior presomitic marker PAX3 (Figures 4C and 4D; no replating). At this point, a subset of the PAX3$^+$ cells (17.5%) coexpressed PAX7, indicating the progression from PAX3$^+$ progenitors to PAX3:PAX7-double positive dermomyotomal-like population (Figures 4C and 4D; no replating). At day 6, the cells emerging from the colony edges expressed PAX3, whereas the cells in the core of the same colony were undifferentiated (KLF4$^+$) (Figure 4B). In

Figure 3. Characterization of human myotubes cultured on Geltrex and laminin coatings

(A) Quantification of the number of nuclei in the myotubes at day 7 cultured on Geltrex- or laminin-coated dishes (n = 3, independent experiments). Error bars, mean ± SEM.

(B) Immunostaining with MYH3, MYH7, MYH8, and DAPI staining in PCi-Myo cells at day 7. Arrowheads indicate nuclei in the myotubes. Scale bar, 60 μM.

(B′) Immunostaining with MYH2, MYH4, MHC, and DAPI staining in PCi-Myo cells at day 7 cultured on laminin-coated dishes. Scale bar, 60 μM.

(C) Immunostaining with DYSTROPHIN, MHC, and DAPI staining in PCi-Myo cells at day 7 cultured on laminin-coated dishes. Scale bar, 60 μM.

(D) MA plot (M (log ratio) and A (mean average)) of PCi-AFR1-derived myotubes on laminin compared to Geltrex RNA-seq data. Significantly dysregulated genes are highlighted in blue (false discovery rate <0.05).

(E) Gene Ontology (GO) analysis for biological processes of the upregulated genes. Selected enriched terms are presented according to the fold enrichment.

(F) Heatmap with the normalized reads per gene of PCi-AFR1-derived-myotubes on laminin and Geltrex RNA-seq data in individual triplicates.

(G) Immunostaining with MHC, ACTN, and DAPI staining in PCi-Myo cells at day 7 of differentiation. Scale bar, 20 μM.

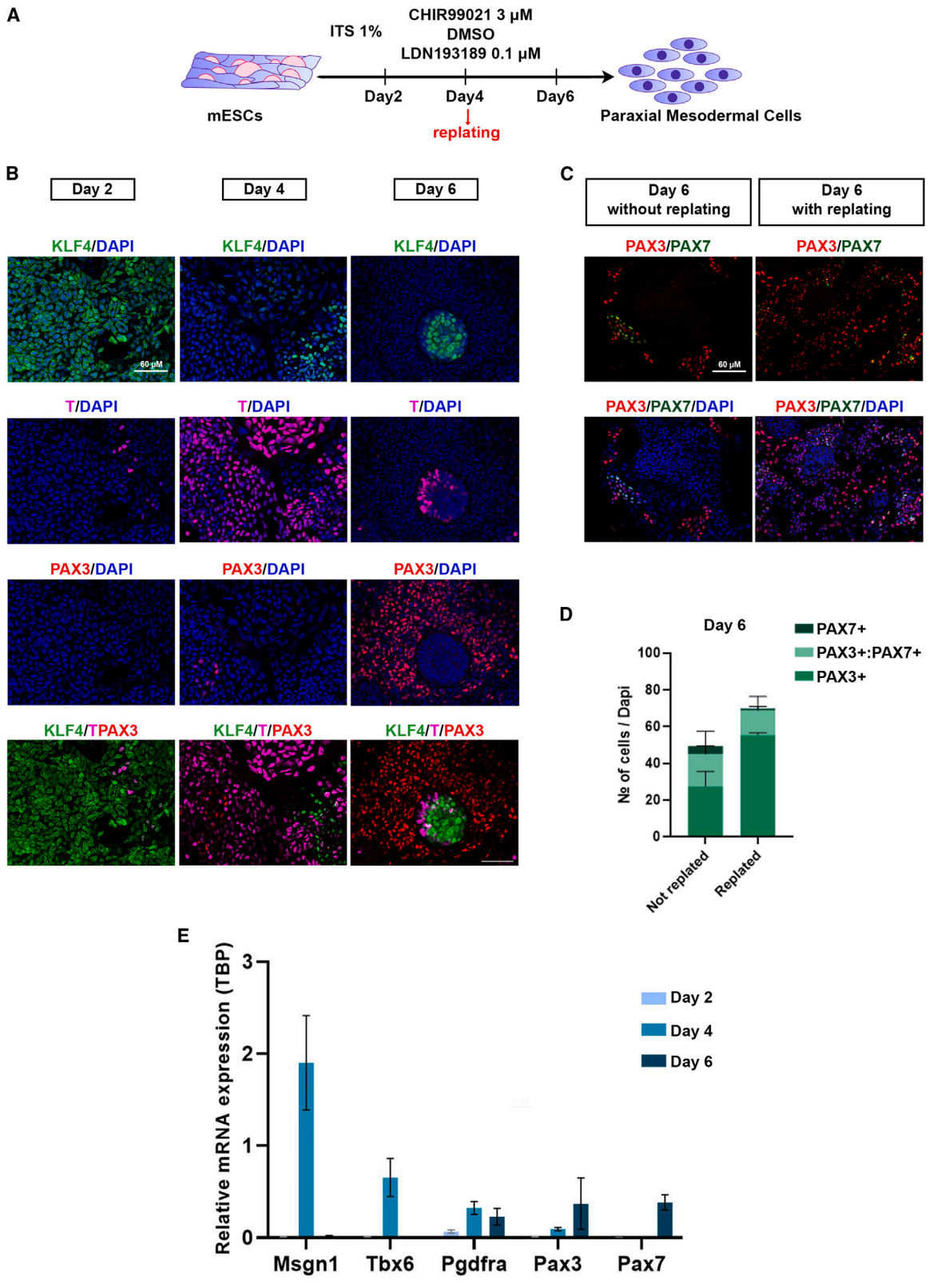

(legend on next page)

between, the cells expressed the early mesodermal marker T (Figure 4B). At day 8, the mESC colonies still expressed the pluripotency factor OCT4, whereas at day 10, the core of the colonies became positive for T, and finally, at day 13, the cells in the colony core became positive for PAX3 (Figures S6A and S6B). This shows that colony differentiation is progressive but follows a myogenic differentiation trajectory. Complete dissociation of the colonies at day 4 and replating at the same density increased cell homogeneity (Figure 4A). This additional step led to an increased number of $PAX3^+$ cells in the entire population (from 31.8% to 54.1%, respectively) at day 6 (Figures 4C′ and 4D). We conclude that the addition of the replating step during paraxial mesodermal differentiation increased the efficiency in generating $PAX3^+$ cells.

Myogenic differentiation of mESC-derived paraxial mesodermal cells

At day 6, paraxial mesodermal progenitors were plated at the optimized confluence of 75,000 cells/cm^2 in maturation medium (Figure 5A). At this stage, the culture is composed of small 3D colonies surrounded by a dense population of isolated cells. After 2 days in maturation medium (day 8), 83.1% (±4.8) of the cells in culture were positive for the muscle progenitor cell markers PAX3 and/or PAX7 (Figures 5B, 5C, S6A, and S6B). We did not detect the expression of the myogenic regulatory factors MYOD or MYOG before day 10 (Figures 5B and S6C). By day 10, we observed cells in 2 distinct differentiation statuses within the isolated cell population: a progenitor zone, containing 28.4% (±2.4) of the cells expressing MYOD (Figures 5B′ and 5C), of which 24% are PAX7:MYOD-double positive and 76% are $MYOD^+$-only (Figure 5E), and a differentiated zone, where 41.8% (±3.4) of the cells expressed MYOG (Figures 5B′ and 5C); of these, 50.3% coexpressed MYOD (Figures 5B′ and 5F). After 13 days in culture (day 13), $MYOD^+$ cells reached 45.3% (±9.5) in the progenitor zone (Figures 5B″ and 5C). Among these, 29% coexpressed $PAX7^+$:$MYOD^+$ (Figure 5E). Moreover, more than 50% of the cells in the differentiated zone expressed MYOG (Figures 5B″ and 5C); of these, 46.4% coexpressed MYOD (Figure 5F). $MYOD^+$:$MYOG^+$ and $MYOG^+$ nuclei could be observed in myosin-expressing myotubes at days 10 and 13 (Figures 5B′ and 5B″). To characterize the myogenic progenitors in the different time points, we dissected the number of $PAX3^+$ and/or $PAX7^+$ cells in these populations (Figure 5D) and complemented the analysis with qRT-PCR (Figure S6D). These results show that the maturation medium can efficiently differentiate mESC-derived paraxial mesodermal cells into the skeletal muscle lineage in 7 days.

Finally, we investigated the myogenic purity in our cultures. Immunostainings showed the absence of adipocytes and endothelial cell markers (Figures S6E and S6E′). qRT-PCR analysis showed an absence in the expression of other-lineage genes in the cultures (Figure 5I). Therefore, we conclude that this protocol provides highly enriched myogenic cell populations from mESCs.

Maturation status of the mESC-derived myogenic fibers

We further examined the maturity state of the myogenic progenitors and myotubes generated using our culture system (Figure 6A). mRNA expression analysis of the cultures shows high expression levels of genes expressed in fetal myoblasts (Biressi et al., 2007a, 2007b), such as *Pkcθ*, *Mck*, *Nfix*, *Jag1*, *Junb* (Figure 6B) and the adult myogenic markers *Itga7* and *Calcr* (Figure 6C). To evaluate the myotube differentiation level, we performed immunostainings for the different MHCs. At day 13, the myotubes were positive for MYH3 (Figure 6D), when cells were replated at day 4. When maintaining the cultures for 3 additional days in maturation medium (day 16), the fetal MYH8 expression was induced (Figure 6D). Notably, we were able to observe MYH8 as early as day 13 if the cells were not replated at day 4 (Figure 6D′). Moreover, when nonreplated at day 4, myotubes cultured up to day 16 expressed the adult slow MYH7 (Figure 6D′).

At day 13, we showed that $PAX7^+$ cells constitute 23.4% (±4.5) of the myogenic population (Figure 5C), and we further observed that these cells are present in close proximity to the myotubes (Figures 6E and 6F), reminiscent of a satellite cell position. Immunostaining for the proliferation marker KI67 revealed that 38.3% of the $PAX7^+$ cells are nonproliferative ($PAX7^+$:$KI67^-$) at day 13, which

Figure 4. Characterization of the paraxial mesodermal cells generated from mESCs

(A) Schematic representation of the experimental time line to generate paraxial mesodermal cells from mESCs.

(B) Immunostaining with KLF4, T, PAX3, and DAPI staining during mESC differentiation into paraxial mesoderm (days 2, 4, and 6). Scale bar, 60 μM.

(C and C′) Immunostaining with PAX3, PAX7, and DAPI staining during mESC differentiation into paraxial mesoderm at day 6, preceded (C′) or not (C) by replating at day 4. Scale bar, 60 μM.

(D) Quantification of the $PAX3^+$:$PAX7^-$, $PAX3^+$:$PAX7^+$, and $PAX7^+$:$PAX3^-$ populations in the whole culture dish of the paraxial mesodermal differentiation at day 6, preceded or not by replating at day 4. Error bars, mean ± SEM.

(E) qRT-PCR analyses of mESCs during paraxial mesodermal differentiation (days 2, 4, and 6) (n = 3, independent experiments). Error bars, mean ± SEM.

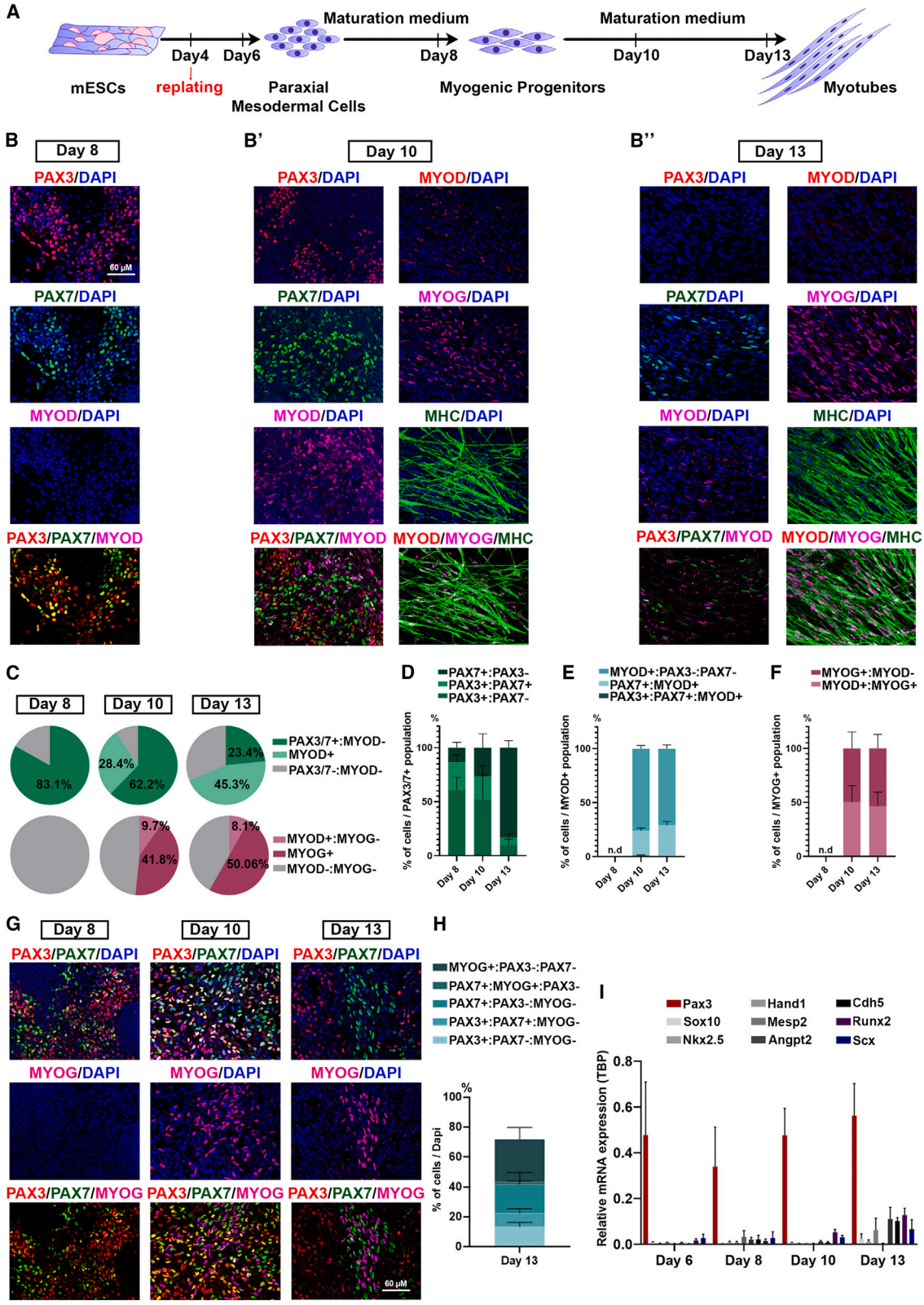

(legend on next page)

suggests the formation of a reserve cell population (Figures 6G and 6H).

The maturation medium drives the commitment of mESC-derived paraxial mesodermal cells into the skeletal muscle lineage with myotube maturation to a mixed fetal and postnatal phenotype and with the formation of reserve cells.

DISCUSSION

Modeling tissue and organ development *in vitro*, through PSC specification, provides the ability to dissect the structural, physiological, and molecular features of organogenesis and obtain a broader knowledge that can be transferred to therapeutic research. Many protocols developed transgene-free approaches to generate skeletal muscle cells from PSCs. However, this directed myogenic differentiation faced several difficulties, such as other lineages contamination, limited generation of high-scale cultures, extended culture time, and poor fiber maturity. The protocol we describe yields a pure myogenic population (PCi-Myo) within 18 days. The PCi-Myo population, composed of $PAX7^+$ and $MYOG^+$ cells, is easily handled, robust in culture, and can be amplified in the amplification medium. When cultured in the maturation medium, the myoblasts generate myotubes with mixed fetal and postnatal phenotypes after 4 days in culture. This is significantly faster than previously published protocols that require more than 30 days in culture to obtain myotubes with similar characteristics (Al Tanoury et al., 2020; Shelton et al., 2016). Our protocol was modified to differentiate hiPSC lines from various backgrounds into a pure population of myogenic cells, making it highly reproducible.

Until recently, the 2D culture system protocols that rely on thestepwise addition of compounds to the culture medium, with the aim of recapitulating developmental stages, did not prevent the presence of nonmyogenic cells in the cultures (Xi et al., 2020). Our protocol is the first to confer a homogeneous myogenic identity to the cell culture that is maintained in differentiation. We show that long-term treatment of hiPSCs with signaling pathway modulators and a novel combination of growth factors (IGF1, FGF2, and heregulin-β-1) with previously defined functions (Chakkalakal et al., 2012; Chargé and Rudnicki, 2004; D'Andrea et al., 2019; Lagha et al., 2008; Sakurai et al., 2009; Wang et al., 2019) allows direct and specific differentiation into the skeletal myogenic lineage. Recently, the long-term application of high concentrations of WNT agonists was shown to induce the formation of dermomyotome-like cells in more than 90% of differentiated hiPSCs (Zhao et al., 2020). This observation is consistent with the long-term exposure effect of the combination of factors seen with our protocol; however, we did not define a dermomyotomal-like population in our experiment. Moreover, proliferation of the PCi-Myo cells was enhanced by removing CHIR99021 and SB431542 and adding forskolin, reported to increase myoblast proliferation (Stewart et al., 2011).

The production of fully mature myotubes *in vitro* is a major hurdle in the development of experimental strategies to produce myogenic cells. Here, we report a culture method that generates human myotubes with a level of maturation

Figure 5. Characterization of the murine skeletal muscle cells generated from mESC-derived paraxial mesodermal cells

(A) Schematic representation of the experimental time line.

(B) Immunostaining with PAX3, PAX7, MYOD, and DAPI staining in mESC-derived paraxial mesodermal cells during differentiation with maturation medium at day 8. Scale bar, 60 μM.

(B′ and B″) Left: immunostaining with PAX3, PAX7, MYOD, and DAPI staining in mESC-derived paraxial mesodermal cells during differentiation with maturation medium at day 10 (B′) and day 13 (B″). Right: immunostaining with MYOD, MYOG, MHC, and DAPI staining in mESC-derived paraxial mesodermal cells during differentiation with maturation medium at day 10 (B′) and day 13 (B″).

(C) Quantification of the cell populations in the whole-cell culture dish during the differentiation of mESC-derived paraxial mesodermal cells with maturation medium (days 8, 10, and 13).

(D) Quantification of the $PAX3^+$:$PAX7^-$, $PAX3^+$:$PAX7^+$ cells, and $PAX7^+$:$PAX3^-$ cells within the $PAX3/7^+$ cell population during the differentiation of mESC-derived paraxial mesodermal cells with maturation medium (days 8, 10, and 13) (n = 3, independent experiments). Error bars, mean ± SEM.

(E and F) Quantification of the (E) $MYOD^+$:$PAX3^-$:$PAX7^-$, $PAX7^+$:$MYOD^+$, and $PAX3^+$:$PAX7^+$:$MYOD^+$ cells within the $MYOD^+$ cell population, and (F) $MYOG^+$:$MYOD^-$ and $MYOD^+$:$MYOG^+$ cells within the $MYOG^+$ cell population during the differentiation of mESC-derived paraxial mesodermal cells with maturation medium (days 8, 10, and 13) (n = 3, independent experiments). n.d., not detected. Error bars, mean ± SEM.

(G) Immunostaining with PAX3, PAX7, MYOG, and DAPI staining in mESC-derived paraxial mesodermal cells during differentiation with maturation medium (days 8, 10, and 13). Scale bar, 60 μM.

(H) Quantification of the cell populations in the whole-cell culture dish at day 13 of the differentiation of mESC-derived paraxial mesodermal cells with maturation medium (n = 3, independent experiments).

(I) qRT-PCR analyses in mESC-derived paraxial mesodermal cells during myogenic differentiation (days 6, 8, 10, and 13) (n = 3, independent experiments). Error bars, mean ± SEM.

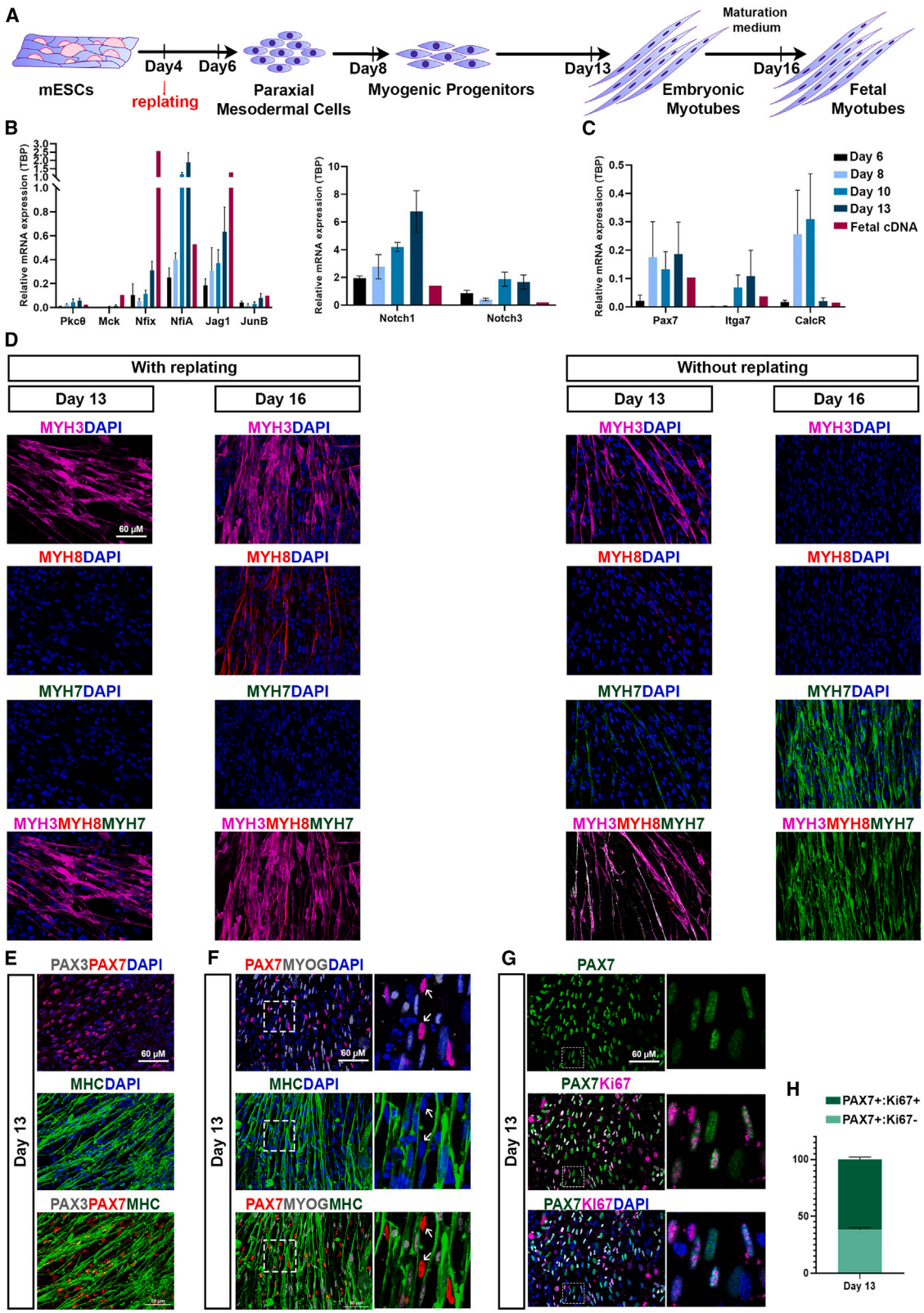

(legend on next page)

comparable to previously published protocols (Caron et al., 2016; Chal et al., 2018; Darabi et al., 2008, 2011; Selvaraj et al., 2019). Achieving a high cell maturity level may require more sophisticated culture systems involving coculture with other cell types such as neuronal (Demestre et al., 2015), endothelial, or immune cells. Moreover, the addition of factors to the cultures, such as those found in the secretome of supportive cells *in vivo* could be explored to improve myotube maturation (Selvaraj et al., 2019). Additional strategies modifying the biophysical status of the culture conditions could also improve the maturity status of the PSC-derived myotubes, such as mimicking the *in vivo* growth matrix (Jiwlawat et al., 2019; Maffioletti et al., 2018).

PSCs maintain a species-specific developmental clock *in vitro* and *in vivo* (Rayon et al., 2020). The delay in differentiation between species was investigated in human and murine ESC neural differentiation, where a higher protein stability and cell-cycle duration was observed in human compared to murine cells (Rayon et al., 2020). Moreover, the oscillation period of the *in vitro* human segmentation clock is between 5 and 6 h, whereas the murine oscillation period varies between 2 and 3 h (Diaz-Cuadros et al., 2020; Matsuda et al., 2020). Although the molecular determinants of the species-specific rates still need to be identified, we also observed distinct time responses between species, during the derivation of myoblasts from hiPSC and mESC, which occurs in 18 and 10 days, respectively, and during human and murine myoblast differentiation, which occurs within 7 and 3 days, respectively.

In this study, we describe an alternative culture method that efficiently generates skeletal muscle cells from hiPSCs and mESCs. The protocol combines the advantages of generating, within a short period of time and without sorting, a pure population of myoblasts that when triggered to differentiate preserves a reserve population. This culture system constitutes a tool for *in vitro* disease modeling and drug screening without the interference of contaminating cell types, which will contribute to improving skeletal muscle research and to discovering new therapeutic opportunities.

EXPERIMENTAL PROCEDURES

Resource availability

Corresponding author

Further information and requests for resources and reagents should be directed to and will be fulfilled by the corresponding author Fréderic Relaix (frederic.relaix@inserm.fr).

Materials availability

This study did not generate new unique reagents. Phenocell maturation medium is available and commercialized at www.phenocell.com/fr.

Data and code availability

Raw and processed data that support the RNA-seq findings were deposited in GEO: GSE240334.

Human iPSCs maintenance and myogenic differentiation

Three undifferentiated hiPSCs (PCi-AFR3, PCi-CAU1, PCi-AFR1; https://www.phenocell.com/) and 1,024 (https://www.istem.eu/en/) lines were cultured on laminin 521–coated dishes in complete mTESR1 medium. hiPSCs were passaged, when 80% confluence was reached as single cells using accutase incubation for 5–10 min at 37°C. Differentiation of the hiPSC lines is found in the supplemental experimental procedures.

Immunocytochemistry

Cultured cells were fixed in 4% paraformaldehyde for 15 min at room temperature and washed in PBS 1×. Immunostaining was performed as previously described (Esteves de Lima et al., 2021). Briefly cells were permeabilized in Triton 0.5% for 10 min and blocked with 5% immunoglobulin G (IgG)–free BSA for 1 h at room temperature. The cells were incubated with primary antibodies (Table S4) and diluted in 5% IgG-free BSA overnight at 4°C. Secondary antibody incubation was performed for 1 h at room temperature followed by DAPI staining (1:5,000) for 10 min at room temperature.

Figure 6. Characterization of the maturity phenotype of the murine myoblasts and myotubes

(A) Schematic representation of the experimental time line.

(B and C) qRT-PCR analyses of mESC-derived paraxial mesodermal cells during myogenic differentiation (days 6, 8, 10, and 13) and in fetal myoblasts (n = 3, independent experiments). Error bars, mean ± SEM.

(D and D′) Immunostaining with MYH3, MYH8, MYH7, and DAPI staining in mESC-derived paraxial mesodermal cells during differentiation with maturation medium, preceded (D) or not (D′) by the replating step at day 4 (days 13 and 16). Scale bar, 60 μM.

(E) Immunostaining with PAX3, PAX7, MHC, and DAPI staining in mESC-derived paraxial mesodermal cells at day 13 of differentiation with maturation medium. Scale bar, 60 μM.

(F) Immunostaining with PAX7, MYOG, MHC, and DAPI staining in mESC-derived paraxial mesodermal cells at day 13 of differentiation with maturation medium. Arrows indicate $PAX7^+$ cells. Scale bar, 60 μM.

(G) Immunostaining with PAX7, KI67, and DAPI staining in mESC-derived paraxial mesodermal cells at day 13 of differentiation with maturation medium. Arrows indicate $PAX7^+$:$KI67^+$ cells and arrowheads indicate $PAX7^+$:$KI67^-$ cells. Scale bar, 60 μM.

(H) Quantification of the $PAX7^+$:$KI67^+$ and $PAX7^+$:$KI67^-$ cells within the $PAX7^+$ cell population at day 13 of myogenic differentiation (n = 3, independent experiments). Error bars, mean ± SEM.

Image capturing and cell quantification

Image capturing was performed using a Zeiss LSM 800 confocal microscope with the associated Zeiss Zen Lite software. Quantifications were performed in samples obtained from 3 independent experiments with at least 5 pictures taken randomly within each sample, using ImageJ (Schneider et al., 2012). All of the data are displayed as mean ± SEM.

RNA extraction, cDNA synthesis, and qRT-PCR

For RNA-seq, 2×10^5 cells were collected per sample, and triplicates were prepared for each condition (MyoB, MyoT on laminin, and MyoT on Geltrex) for RNA extraction (Macherey Nagel, 740955) following the manufacturer's protocol. For qRT-PCR, a minimum of 2×10^5 cells were collected per sample for RNA extraction using the same kit. Reverse transcription was performed using the SuperScript III Reverse Transcriptase following the manufacturer's guidelines. qRT-PCR was performed using the PowerUp SYBR Green Master Mix. The relative mRNA levels were calculated using the $2^{\Delta\Delta Ct}$ method (Livak and Schmittgen, 2001). The ΔCt were obtained from Ct normalized to the housekeeping gene *Tbp* levels in each sample. The qRT-PCR primers used are listed in Tables S2 and S3.

RNA-seq

RNA was prepared as described above and sent to the IMRB (Institut Mondor de Recherche Biomédicale) genomic platform. Libraries were prepared with the TruSeq Stranded Total RNA Sample preparation kit according to supplier recommendations. Briefly, the key stages of this protocol are successively the removal of rRNA fractions from 1 μg of total RNA using the Ribo-Zero Gold Kit; fragmentation using divalent cations under elevated temperature to obtain approximately 300-bp pieces; double-stranded cDNA synthesis using RT and random primers; and Illumina adapter ligation and cDNA library amplification by PCR for sequencing. Sequencing was carried out on single-end 75 bp of Illumina NextSeq500.

Flow cytometry analysis

PCi-AFR1/1024/PCi-Cau1/PCi-AFR3-derived myoblasts were incubated with CDH13-FITC, HGFR/c-MET-APC, and erbB3/HER-3-PE antibodies (Table S4) for 30 min on ice protected from light. Compensation beads (BD CompBeads, BD Biosciences, catalog no. 552843) were used for initial compensation setup and fluorescence minus one controls were used to determine the background level of each fluorochrome. Analyses were performed on BD LSR Fortessa X-20 using BD FACS Diva Software version 8 (BD Biosciences) and results were analyzed using FlowJo software version 10.5.3.

Statistical analysis

Quantifications were performed in at least 5 pictures taken randomly within each sample per experiment, and statistics were done with GraphPad Prism version 8 and Microsoft Excel. The statistical test performed in each analysis is described in the associated figure legend.

SUPPLEMENTAL INFORMATION

Supplemental information can be found online at https://doi.org/10.1016/j.stemcr.2023.11.002.

ACKNOWLEDGMENTS

We thank lab members for reading and commenting on the manuscript. We thank Stéphane Kerbrat from the IMRB genomic platform. We thank Aurélie Guguin from the IMRB cytometry platform. We thank the animal facilities EP3 from IMRB and TAAM from CDTA. We thank Nassim-Anis Ahmine for the acquisition of the α-actinin immunostainings. We thank Chafic Abou Akar for the illustrations. The Relaix lab receives funding from Association Française contre les Myopathies (AFM) via TRANSLAMUSCLE (PROJECT 19507 and 22946), Labex REVIVE (ANR-10-LABX-73), Agence Nationale pour la Recherche (ANR) grant Satnet (ANR-15-CE13-0011-01), BMP-MyoStem (ANR-16-CE14-0002-03), MyoStemVasc (ANR-17-CE14-0018-01), and FRM (EQU202003010217).

AUTHOR CONTRIBUTIONS

R.B.A. performed and analyzed most of the experiments. C.L., D.A., J.M., B.O., and J.E.d.L. performed and analyzed the experiments. J.E.d.L. performed the bioinformatic analysis. J.E.d.L. and F.R. designed, supervised, and oversaw the project. R.B.A., J.E.d.L., and F.R. wrote the manuscript.

DECLARATION OF INTERESTS

R.B.A., C.L., J.E.d.L., and F.R. declare no competing interests. D.A., J.M., and B.O. work or have worked for Phenocell.

Received: January 4, 2023
Revised: November 14, 2023
Accepted: November 15, 2023
Published: December 14, 2023

REFERENCES

Abujarour, R., Bennett, M., Valamehr, B., Lee, T.T., Robinson, M., Robbins, D., Le, T., Lai, K., and Flynn, P. (2014). Myogenic Differentiation of Muscular Dystrophy-Specific Induced Pluripotent Stem Cells for Use in Drug Discovery. STEM CELLS Transl. *3*, 149–160.

Akiyama, T., Sato, S., Chikazawa-Nohtomi, N., Soma, A., Kimura, H., Wakabayashi, S., Ko, S.B.H., and Ko, M.S.H. (2018). Efficient differentiation of human pluripotent stem cells into skeletal muscle cells by combining RNA-based MYOD1-expression and POU5F1-silencing. Sci. Rep. *8*, 1189.

Al Tanoury, Z., Rao, J., Tassy, O., Gobert, B., Gapon, S., Garnier, J.-M., Wagner, E., Hick, A., Hall, A., Gussoni, E., and Pourquié, O. (2020). Differentiation of the human PAX7-positive myogenic precursors/satellite cell lineage *in vitro*. Development *147*, dev187344.

Albini, S., Coutinho, P., Malecova, B., Giordani, L., Savchenko, A., Forcales, S.V., and Puri, P.L. (2013). Epigenetic Reprogramming of Human Embryonic Stem Cells into Skeletal Muscle Cells and Generation of Contractile Myospheres. Cell Rep. *3*, 661–670.

Barbet, J.P., Thornell, L.-E., and Butler-Browne, G.S. (1991). Immunocytochemical characterisation of two generations of fibers

during the development of the human quadriceps muscle. Mech. Dev. *35*, 3–11.

Biressi, S., Molinaro, M., and Cossu, G. (2007a). Cellular heterogeneity during vertebrate skeletal muscle development. Dev. Biol. *308*, 281–293.

Biressi, S., Tagliafico, E., Lamorte, G., Monteverde, S., Tenedini, E., Roncaglia, E., Ferrari, S., Ferrari, S., Cusella-De Angelis, M.G., Tajbakhsh, S., and Cossu, G. (2007b). Intrinsic phenotypic diversity of embryonic and fetal myoblasts is revealed by genome-wide gene expression analysis on purified cells. Dev. Biol. *304*, 633–651.

Buckingham, M., and Rigby, P.W.J. (2014). Gene Regulatory Networks and Transcriptional Mechanisms that Control Myogenesis. Dev. Cell *28*, 225–238.

Caron, L., Kher, D., Lee, K.L., McKernan, R., Dumevska, B., Hidalgo, A., Li, J., Yang, H., Main, H., Ferri, G., et al. (2016). A Human Pluripotent Stem Cell Model of Facioscapulohumeral Muscular Dystrophy-Affected Skeletal Muscles. STEM CELLS Transl. Med. *5*, 1145–1161.

Chakkalakal, J.V., Jones, K.M., Basson, M.A., and Brack, A.S. (2012). The aged niche disrupts muscle stem cell quiescence. Nature *490*, 355–360.

Chal, J., Al Tanoury, Z., Oginuma, M., Moncuquet, P., Gobert, B., Miyanari, A., Tassy, O., Guevara, G., Hubaud, A., Bera, A., et al. (2018). Recapitulating early development of mouse musculoskeletal precursors of the paraxial mesoderm *in vitro*. Development *145*, dev157339.

Chal, J., Oginuma, M., Al Tanoury, Z., Gobert, B., Sumara, O., Hick, A., Bousson, F., Zidouni, Y., Mursch, C., Moncuquet, P., et al. (2015). Differentiation of pluripotent stem cells to muscle fiber to model Duchenne muscular dystrophy. Nat. Biotechnol. *33*, 962–969.

Chargé, S.B.P., and Rudnicki, M.A. (2004). Cellular and Molecular Regulation of Muscle Regeneration. Physiol. Rev. *84*, 209–238.

Cho, M., Webster, S.G., and Blau, H.M. (1993). Evidence for myoblast-extrinsic regulation of slow myosin heavy chain expression during muscle fiber formation in embryonic development. J. Cell Biol. *121*, 795–810.

Choi, I.Y., Lim, H., Estrellas, K., Mula, J., Cohen, T.V., Zhang, Y., Donnelly, C.J., Richard, J.-P., Kim, Y.J., Kim, H., et al. (2016). Concordant but Varied Phenotypes among Duchenne Muscular Dystrophy Patient-Specific Myoblasts Derived using a Human iPSC-Based Model. Cell Rep. *15*, 2301–2312.

D'Andrea, P., Sciancalepore, M., Veltruska, K., Lorenzon, P., and Bandiera, A. (2019). Epidermal Growth Factor – based adhesion substrates elicit myoblast scattering, proliferation, differentiation and promote satellite cell myogenic activation. Biochim. Biophys. Acta BBA - Mol. Cell Res. *1866*, 504–517.

Darabi, R., Gehlbach, K., Bachoo, R.M., Kamath, S., Osawa, M., Kamm, K.E., Kyba, M., and Perlingeiro, R.C.R. (2008). Functional skeletal muscle regeneration from differentiating embryonic stem cells. Nat. Med. *14*, 134–143.

Darabi, R., Pan, W., Bosnakovski, D., Baik, J., Kyba, M., and Perlingeiro, R.C.R. (2011). Functional myogenic engraftment from mouse iPS cells. Stem Cell Rev. Rep. *7*, 948–957.

Dekel, I., Magal, Y., Pearson-White, S., Emerson, C., and Shani, M. (1992). Conditional conversion of ES cells to skeletal muscle by an exogenous MyoD1 gene. New Biol. *4*, 217–224.

Demestre, M., Orth, M., Föhr, K.J., Achberger, K., Ludolph, A.C., Liebau, S., and Boeckers, T.M. (2015). Formation and characterisation of neuromuscular junctions between hiPSC derived motoneurons and myotubes. Stem Cell Res. *15*, 328–336.

Diaz-Cuadros, M., Wagner, D.E., Budjan, C., Hubaud, A., Tarazona, O.A., Donelly, S., Michaut, A., Al Tanoury, Z., Yoshioka-Kobayashi, K., Niino, Y., et al. (2020). In vitro characterization of the human segmentation clock. Nature *580*, 113–118.

Draeger, A., Weeds, A.G., and Fitzsimons, R.B. (1987). Primary, secondary and tertiary myotubes in developing skeletal muscle: A new approach to the analysis of human myogenesis. J. Neurol. Sci. *81*, 19–43.

Ecob-Prince, M., Hill, M., and Brown, W. (1989). Immunocytochemical demonstration of myosin heavy chain expression in human muscle. J. Neurol. Sci. *91*, 71–78.

Esteves de Lima, J., Bonnin, M.-A., Bourgeois, A., Parisi, A., Le Grand, F., and Duprez, D. (2014). Specific pattern of cell cycle during limb fetal myogenesis. Dev. Biol. *392*, 308–323.

Esteves de Lima, J., Bou Akar, R., Machado, L., Li, Y., Drayton-Libotte, B., Dilworth, F.J., and Relaix, F. (2021). HIRA stabilizes skeletal muscle lineage identity. Nat. Commun. *12*, 3450.

Esteves de Lima, J., and Relaix, F. (2021). Master regulators of skeletal muscle lineage development and pluripotent stem cells differentiation. Cell Regen. *10*, 31.

Hicks, M.R., Hiserodt, J., Paras, K., Fujiwara, W., Eskin, A., Jan, M., Xi, H., Young, C.S., Evseenko, D., Nelson, S.F., et al. (2018). ERBB3 and NGFR mark a distinct skeletal muscle progenitor cell in human development and hPSCs. Nat. Cell Biol. *20*, 46–57.

Jiwlawat, N., Lynch, E.M., Napiwocki, B.N., Stempien, A., Ashton, R.S., Kamp, T.J., Crone, W.C., and Suzuki, M. (2019). Micropatterned substrates with physiological stiffness promote cell maturation and Pompe disease phenotype in human induced pluripotent stem cell-derived skeletal myocytes. Biotechnol. Bioeng. *116*, 2377–2392.

Lagha, M., Kormish, J.D., Rocancourt, D., Manceau, M., Epstein, J.A., Zaret, K.S., Relaix, F., and Buckingham, M.E. (2008). Pax3 regulation of FGF signaling affects the progression of embryonic progenitor cells into the myogenic program. Genes Dev. *22*, 1828–1837.

Livak, K.J., and Schmittgen, T.D. (2001). Analysis of Relative Gene Expression Data Using Real-Time Quantitative PCR and the $2^{-\Delta\Delta CT}$ Method.Pdf.

Maffioletti, S.M., Sarcar, S., Henderson, A.B.H., Mannhardt, I., Pinton, L., Moyle, L.A., Steele-Stallard, H., Cappellari, O., Wells, K.E., Ferrari, G., et al. (2018). Three-Dimensional Human iPSC-Derived Artificial Skeletal Muscles Model Muscular Dystrophies and Enable Multilineage Tissue Engineering. Cell Rep. *23*, 899–908.

Matsuda, M., Yamanaka, Y., Uemura, M., Osawa, M., Saito, M.K., Nagahashi, A., Nishio, M., Guo, L., Ikegawa, S., Sakurai, S., et al. (2020). Recapitulating the human segmentation clock with pluripotent stem cells. Nature *580*, 124–129.

Messina, G., Biressi, S., Monteverde, S., Magli, A., Cassano, M., Perani, L., Roncaglia, E., Tagliafico, E., Starnes, L., and Campbell, C.E. (2010). Nfix Regulates Fetal-Specific Transcription in Developing Skeletal Muscle. Cell *140*, 554–566.

Messina, G., and Cossu, G. (2009). The origin of embryonic and fetal myoblasts: a role of Pax3 and Pax7. Genes Dev. *23*, 902–905.

Nalbandian, M., Zhao, M., Sasaki-Honda, M., Jonouchi, T., Lucena-Cacace, A., Mizusawa, T., Yasuda, M., Yoshida, Y., Hotta, A., and Sakurai, H. (2021). Characterization of hiPSC-Derived Muscle Progenitors Reveals Distinctive Markers for Myogenic Cell Purification Toward Cell Therapy. Stem Cell Rep. *16*, 883–898.

Picard, C.A., and Marcelle, C. (2013). Two distinct muscle progenitor populations coexist throughout amniote development. Dev. Biol. *373*, 141–148.

Rayon, T., Stamataki, D., Perez-Carrasco, R., Garcia-Perez, L., Barrington, C., Melchionda, M., Exelby, K., Lazaro, J., Tybulewicz, V.L.J., Fisher, E.M.C., and Briscoe, J. (2020). Species-specific pace of development is associated with differences in protein stability. Science *369*, eaba7667.

Sakurai, H., Inami, Y., Tamamura, Y., Yoshikai, T., Sehara-Fujisawa, A., and Isobe, K.-I. (2009). Bidirectional induction toward paraxial mesodermal derivatives from mouse ES cells in chemically defined medium. Stem Cell Res. *3*, 157–169.

Sato, T., Higashioka, K., Sakurai, H., Yamamoto, T., Goshima, N., Ueno, M., and Sotozono, C. (2019). Core Transcription Factors Promote Induction of PAX3-Positive Skeletal Muscle Stem Cells. Stem Cell Rep. *13*, 352–365.

Schiaffino, S., Rossi, A.C., Smerdu, V., Leinwand, L.A., and Reggiani, C. (2015). Developmental myosins: expression patterns and functional significance. Skelet. Muscle *5*, 22.

Schneider, C.A., Rasband, W.S., and Eliceiri, K.W. (2012). NIH Image to ImageJ: 25 years of image analysis. Nat. Methods *9*, 671–675.

Selvaraj, S., Mondragon-Gonzalez, R., Xu, B., Magli, A., Kim, H., Lainé, J., Kiley, J., Mckee, H., Rinaldi, F., Aho, J., et al. (2019). Screening identifies small molecules that enhance the maturation of human pluripotent stem cell-derived myotubes. Elife *8*, e47970.

Shelton, M., Kocharyan, A., Liu, J., Skerjanc, I.S., and Stanford, W.L. (2016). Robust generation and expansion of skeletal muscle progenitors and myocytes from human pluripotent stem cells. Methods *101*, 73–84.

Shevde, N.K., and Mael, A.A. (2013). Techniques in embryoid body formation from human pluripotent stem cells. Methods Mol. Biol. Clifton NJ *946*, 535–546.

Stewart, R., Flechner, L., Montminy, M., and Berdeaux, R. (2011). CREB Is Activated by Muscle Injury and Promotes Muscle Regeneration. PLoS One *6*, e24714.

Tanaka, A., Woltjen, K., Miyake, K., Hotta, A., Ikeya, M., Yamamoto, T., Nishino, T., Shoji, E., Sehara-Fujisawa, A., Manabe, Y., et al. (2013). Efficient and Reproducible Myogenic Differentiation from Human iPS Cells: Prospects for Modeling Miyoshi Myopathy In Vitro. PLoS One *8*, e61540.

Tedesco, F.S., Gerli, M.F.M., Perani, L., Benedetti, S., Ungaro, F., Cassano, M., Antonini, S., Tagliafico, E., Artusi, V., Longa, E., et al. (2012). Transplantation of Genetically Corrected Human iPSC-Derived Progenitors in Mice with Limb-Girdle Muscular Dystrophy. Sci. Transl. Med. *4*, 140ra89.

Wang, Y.X., Feige, P., Brun, C.E., Hekmatnejad, B., Dumont, N.A., Renaud, J.-M., Faulkes, S., Guindon, D.E., and Rudnicki, M.A. (2019). EGFR-Aurka Signaling Rescues Polarity and Regeneration Defects in Dystrophin-Deficient Muscle Stem Cells by Increasing Asymmetric Divisions. Cell Stem Cell *24*, 419–432.e6.

Warren, L., Manos, P.D., Ahfeldt, T., Loh, Y.-H., Li, H., Lau, F., Ebina, W., Mandal, P.K., Smith, Z.D., Meissner, A., et al. (2010). Highly Efficient Reprogramming to Pluripotency and Directed Differentiation of Human Cells with Synthetic Modified mRNA. Cell Stem Cell *7*, 618–630.

Xi, H., Langerman, J., Sabri, S., Chien, P., Young, C.S., Younesi, S., Hicks, M., Gonzalez, K., Fujiwara, W., Marzi, J., et al. (2020). A Human Skeletal Muscle Atlas Identifies the Trajectories of Stem and Progenitor Cells across Development and from Human Pluripotent Stem Cells. Cell Stem Cell *27*, 158–176.e10.

Zhao, M., Tazumi, A., Takayama, S., Takenaka-Ninagawa, N., Nalbandian, M., Nagai, M., Nakamura, Y., Nakasa, M., Watanabe, A., Ikeya, M., et al. (2020). Induced Fetal Human Muscle Stem Cells with High Therapeutic Potential in a Mouse Muscular Dystrophy Model. Stem Cell Rep. *15*, 80–94.